Earth and Planetary Science Letters 614 (2023) 118189

Contents lists available at ScienceDirect

Earth and Planetary Science Letters

journal homepage: www.elsevier.com/locate/epsl

Magmatism during the continent – ocean transition

Tyrone O. Rooney [a,*], Eric L. Brown [b], Ian D. Bastow [c], J Ramón Arrowsmith [d], Christopher J. Campisano [e]

[a] Dept. of Earth and Environmental Sciences, Michigan State University, East Lansing, MI 48824, USA
[b] Dept. of Geoscience, Aarhus University, Denmark
[c] Department of Earth Science and Engineering, Imperial College London, London, UK
[d] School of Earth and Space Exploration, Arizona State University, Tempe, AZ 85287, USA
[e] School of Human Evolution and Social Change and the Institute of Human Origins, Arizona State University, Tempe, AZ 85287, USA

ARTICLE INFO

Article history:
Received 29 July 2022
Received in revised form 24 March 2023
Accepted 21 April 2023
Available online xxxx
Editor: R. Hickey-Vargas

Keywords:
rifting
East Africa
Afar Stratoid Series
magmatism

ABSTRACT

As continents break apart, the dominant mechanism of extension transitions from faulting and lithospheric stretching to magma intrusion and oceanic crust formation in a new ocean basin. A common feature of this evolution preserved at magmatic rifted margins worldwide are voluminous lava flows that erupted close to sea level during the final stages of development of the continent-ocean transition (COT). The mechanisms responsible for the generation of the melts that contribute to these voluminous flows, the so-called seaward dipping reflectors (SDR), and their significance in the context of COT development, are relatively poorly understood; they lie deep below post-rift strata along submarine rifted margins where they cannot be studied directly. Extensive coring of the Afar Stratoid Series - an areally-extensive sequence of Pliocene-aged basalts and intercalated sediments that lie atop the developing COT in the sub-aerial Afar Depression, northern Ethiopia - offers fresh scope to address this issue. We present a numerical model simulating the formation of enriched metasomes within the continental lithospheric mantle by the passage of magmas resembling modern axial basalts. Thermal destabilization of the metasome, caused by plate stretching, initiates melt formation within the metasome. These melts, when mixed with a depleted lithospheric mantle component, closely match the range of compositions of the Afar Stratoid Series lavas in this study. Metasomatic re-enrichment and subsequent melting of the lithospheric mantle during the COT may contribute to further plate thinning. These results demonstrate a novel mechanism by which large-volume flows may be erupted during the COT.

1. Introduction

When continents break apart, faulting, diking, and stretching of initially-thick continental lithosphere eventually gives way to the formation of new oceanic crust at a mid ocean ridge spreading center. The transition between these two fundamentally different styles of strain accommodation occurs in the highly attenuated lithosphere of mature continental rifts – typically preserved as the basement of rifted margins (e.g., Eldholm et al., 2000; Whitmarsh et al., 2001; Menzies et al., 2002). Insights derived from the study of both in situ (e.g., Pérez-Gussinyé and Reston, 2001; Peron-Pinvidic et al., 2013; Brune et al., 2017) and uplifted rifted margins (e.g., Manatschal and Müntener, 2009; Müntener et al., 2010) has resulted in the recognition of two broad endmembers – magma-poor and magma-rich rifted margins (e.g., Franke, 2013; Peron-Pinvidic et al., 2019).

A ubiquitous feature of magma-rich rifted plate margins worldwide are the large volumes of extrusive igneous rock that drape over the continent-ocean transition (COT). These 'seaward dipping reflectors' (SDRs) – sequences of sediments and basalts typically imaged in seismic reflection profiles, are generally thought to have been emplaced immediately before the onset of oceanic spreading, while the young rifted margins were still close to sea level (e.g., Holbrook and Kelemen, 1993). The common occurrence of SDRs within the continent-ocean transition, but their absence within mature ocean basins, suggests SDR magma generation processes are an important component of the active tectonic processes during the final stages of rupture of the continental lithosphere. However, the processes that operated during COT development at continental margins have long-since ceased, and SDRs are typically buried under thick post-rift sediments (e.g., Hinz et al., 1999). This

* Corresponding author.
E-mail address: rooneyt@msu.edu (T.O. Rooney).

https://doi.org/10.1016/j.epsl.2023.118189
0012-821X/

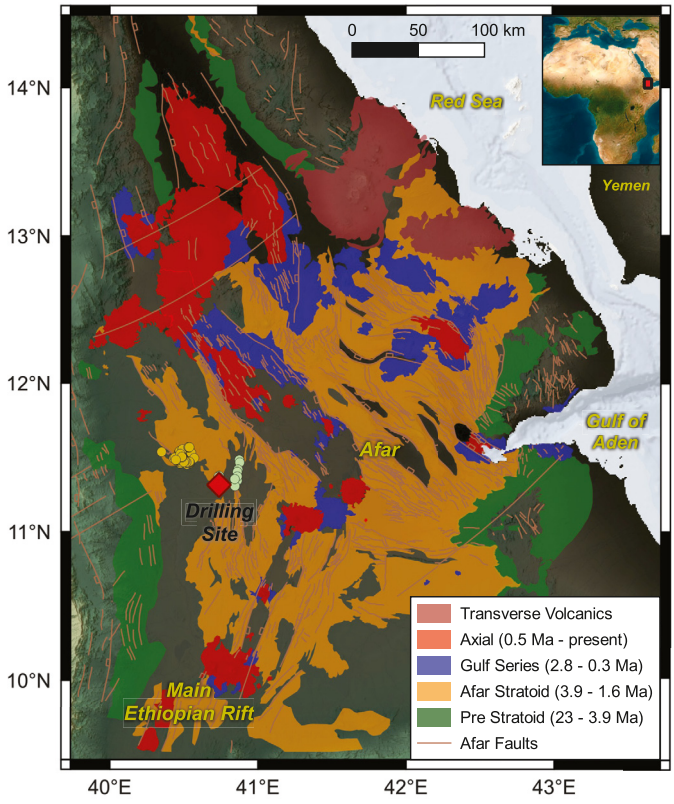

Fig. 1. Distribution of magmatic activity in Afar based upon existing work (Le Gall et al., 2015; Stab et al., 2016; Varet, 2017; Rooney, 2020a). The pre-Stratoid field incorporates the mapped extent of the Dalha Series (10 Ma – 5.6 Ma), and earlier Miocene undifferentiated (10 – 23 Ma). Note that the Dalhoid Series (5.6 – 3.9 Ma) is typically mapped as either part of the Dalha or Stratoid Series and thus is not shown as a discrete unit. The two HSPDP drill sites are located in the area highlighted by the red diamond. The location of the 'outcrop' samples are shown by the aquamarine circles. 'Regional' samples are shown by a yellow circle.

makes them largely inaccessible, and their melt generation mechanisms uncertain.

Existing insights into processes of melt generation during the COT are largely based on results of ocean drilling undertaken on the margins of the North Atlantic (e.g., Fitton et al., 1998), where melt volumes exceed that possible through passive upwelling of the upper mantle. Increased melt volumes were interpreted as resulting from the active fluxing of plume material with elevated mantle potential temperatures into the melting regions (e.g., Fitton et al., 2000; Holbrook et al., 2001). Given the lack of parallel datasets from other rifted margins, however, it remains unclear whether this model is broadly applicable to magma generation processes during the COT.

Tectonically active Afar, within the northern East African Rift, is the best location globally in which to study magmatic rift development and processes of the COT sub-aerially without the masking effects of post-rift thermal subsidence and sedimentation (Fig. 1). In Afar, transition is under way between plate extension processes modulated by lithospheric thinning and those controlled by magma intrusion (e.g., Bastow and Keir, 2011). Within the rift, extensional strain has localized into 60 km-long, 20 km-wide Quaternary magmatic segments, leading to the suggestion that the observed shift to extension by magma intrusion is the final one prior to the onset of spreading at a new mid-ocean ridge and localization of the plate boundary (e.g., Ebinger and Casey, 2001). The Afar Stratoid Series, a Pliocene group of sub-aerially extensive basaltic flows that crop out broadly throughout Afar (Fig. 1), may provide an explanation and analogue as to how large volume flows are emplaced during the COT. Relatively slow extension rates in Afar, coupled with the observation that crustal thinning is lacking across most of the Depression (Ebinger et al., 2017) means melt generation via stretching-related decompression melting of asthenosphere is not a mechanism that can be readily invoked to explain melt pulses across the such a broad region. The existing models describing the formation of large volumes of melt during the COT cannot easily explain the formation of the Afar Stratoid Series. The Afar Stratoid Series is underlain by a 500-km-wide slow wavespeed mantle anomaly (e.g., Ritsema et al., 2011), interpreted as the African Superplume, which is thought to have shaped the region since ~45 Ma ago (Ebinger and Sleep, 1998). Thus, a hypothesis of Afar Stratoid Series formation by active fluxing of plume material into a localized melting zone, during just this specific episode of magmatism, is not readily supported. Alternative melt generation mechanisms must therefore be investigated.

Here we present a geochemical study of a suite of stratigraphically constrained Afar Stratoid Series basalts that were cored as part of the Hominin Sites and Paleolakes Drilling Project (Cohen et al., 2016; Campisano et al., 2017). We show that the geochemical characteristics of these lavas differ substantially from Quaternary axial lavas, requiring a different mode of melt generation. Using a hydrous metasome formation and melting model (Pilet et al., 2011), we test the hypothesis that the Afar Stratoid Series lavas are derived from melting of a lithospheric mantle that has been metasomatically enriched by the passage of recent plume-related magmas. We show that perturbation of the geotherm, for example caused by a period of lithospheric thinning prior to the eruption of the Afar Stratoid Series, can destabilize and melt the enriched lithospheric mantle. Our study shows that re-enrichment and subsequent thermal destabilization of the continental lithospheric mantle may represent an important melt generation mechanism during the COT.

2. Background

2.1. Magmatism during the continent-ocean transition

SDRs are a seismically-defined feature of many magmatic margins globally. They comprise intercalations of sub-aerially erupted basalts and sediment deposited along the continent-ocean transition (e.g., Franke, 2013). Early models attributed SDRs to late-stage rift volcanism that was generated by rapid upwelling of either normal asthenosphere following focused extension (e.g., Mutter et al., 1988) or decompression melting of plume-influenced upper mantle (e.g., White et al., 1987; Fitton et al., 1998, 2000). Recent work suggests the necessity for elevated mantle potential temperatures to form SDRs (Paton et al., 2017). However, SDRs can extend thousands of kilometers along the strike of rifted margins, suggesting that a tectonic, and not solely a hotspot-related mechanism of formation is likely (Gallahue et al., 2020). Given the observation of lithospheric mantle re-fertilization and enrichment during rifting (e.g., Baker et al., 1998; Müntener et al., 2010), and the common occurrence of rift magmas derived from melts of enriched continental lithospheric mantle (e.g., Rooney, 2020b), we suggest that melting of enriched lithospheric mantle may play a role in the generation of SDRs.

2.2. Cenozoic magmatism of East Africa

The Cenozoic magmatic activity of East Africa results from the interaction between the African Superplume and the East African upper mantle and lithosphere (e.g., Furman et al., 2006; Rooney, 2020b). Mantle potential temperatures have been elevated throughout the Cenozoic (Rooney et al., 2012b), contributing to melt generation processes, but melting of enriched lithospheric mantle has also been important during rift development (e.g., Nelson et al., 2019). Large-scale magmatism commenced ca. 45 Ma

with flood basalts centered on southern Ethiopia and northern Kenya (e.g., Rooney, 2017). Over the next 15 Ma, magmatism expanded northward, culminating in the Oligocene flood basalts of the northwest Ethiopian Plateau (e.g., Pik et al., 1999). Following the Eocene-Oligocene plume-lithosphere interaction, a new Early Miocene pulse of volumetrically much less significant, but widely distributed magmatism attributed to lithospheric destabilization, is evident throughout East Africa (Rooney, 2017). Following this period, magmatism became increasingly bi-modal in composition and focused on the evolving Eastern and Western Branches of the East African Rift System (Rooney, 2020b). Modern volcanism in the EARS extends from the highly alkaline products near to the Tanzania Craton (e.g., Rogers et al., 1998) to subalkaline basalts and rhyolites in the well-developed rifting of the Afar Depression (e.g., Alene et al., 2017; Feyissa et al., 2019).

2.3. Afar

Afar represents the mature northern end of the Eastern Branch of the East African Rift System, where the continental crust thins from ~30 km to <15 km (e.g., Bastow and Keir, 2011; Ebinger et al., 2017). During the initial development of the rift margin from ca. 20 to 10 Ma, magmatism in Afar was largely rhyolitic with subordinate basalts (Mablas Series) (Fig. 1) (Varet, 2017). Coincident with the development of rift-marginal basins a new phase of magmatic activity impacted Afar: the Dalha Series are dominantly crustally contaminated basalts occurring around the margins of Afar from ca. 10 Ma to 5.6 Ma (Varet, 2017; Rooney, 2020a). The basaltic Dalhoid Series continued episodically from 5.6 to 3.9 Ma, also occurring around the margins of Afar (Rooney, 2020a). The most significant magmatic event in the region is the eruption of the widespread Afar Stratoid series, which commenced ca. 3.9 Ma and covers much of the basin (55,000 km^2) (e.g., Lahitte et al., 2003). Subsequent magmatism of the Gulf Series and Axial Series is far more spatially restricted (Fig. 1) and linked with the evolving zones of focused magmatic-tectonic intrusion (Lahitte et al., 2003; Le Gall et al., 2015).

3. Methods

The Hominin Sites and Paleolakes Drilling Project (HSPDP), which penetrated thick lava flows of the Afar Stratoid Series and associated sediments in the Northern Afar (Cohen et al., 2016; Campisano et al., 2017), provides an opportunity to examine the relationship between the basaltic flows and associated sediments during the Pliocene. The HSPDP drill core in Afar comprises core material recovered from two sites (NAO and NAW) ~3 km apart, and reveals ~270 m of the composite stratigraphy (Fig. 2). The age range of the material sampled is between ca. 2.9 Ma and 3.3 Ma. Within the cores, seven distinct basaltic horizons were recorded, with thicknesses of 9-38 m. Between these basaltic units, sedimentary horizons were dominantly lacustrine, with evidence of episodic, subaerial exposure and are correlative with the Hadar Formation (ca. 2.9-3.8 Ma: DiMaggio et al., 2015; Rooney, 2020a). This seven-fold division has been expanded to ten basalts given the geochemical evidence. Each expanded basalt horizon is termed an 'interval' within this contribution. Intervals 1 and 2 are from core NAO, while intervals 3–10 are from core NAW (Fig. 2). Multiple samples from each interval were taken from the core. A selection of hand samples were taken from outcrops of basaltic flows surrounding the two drill sites to a maximum distance of ~24 km.

All intervals within the core exhibit intergranular texture, with the exception of Interval 1 (sub-ophitic). Glomeroporphyritic texture is evident throughout the core, manifesting as amalgamations of larger plagioclase and small clinopyroxene. Glomeroporphyritic

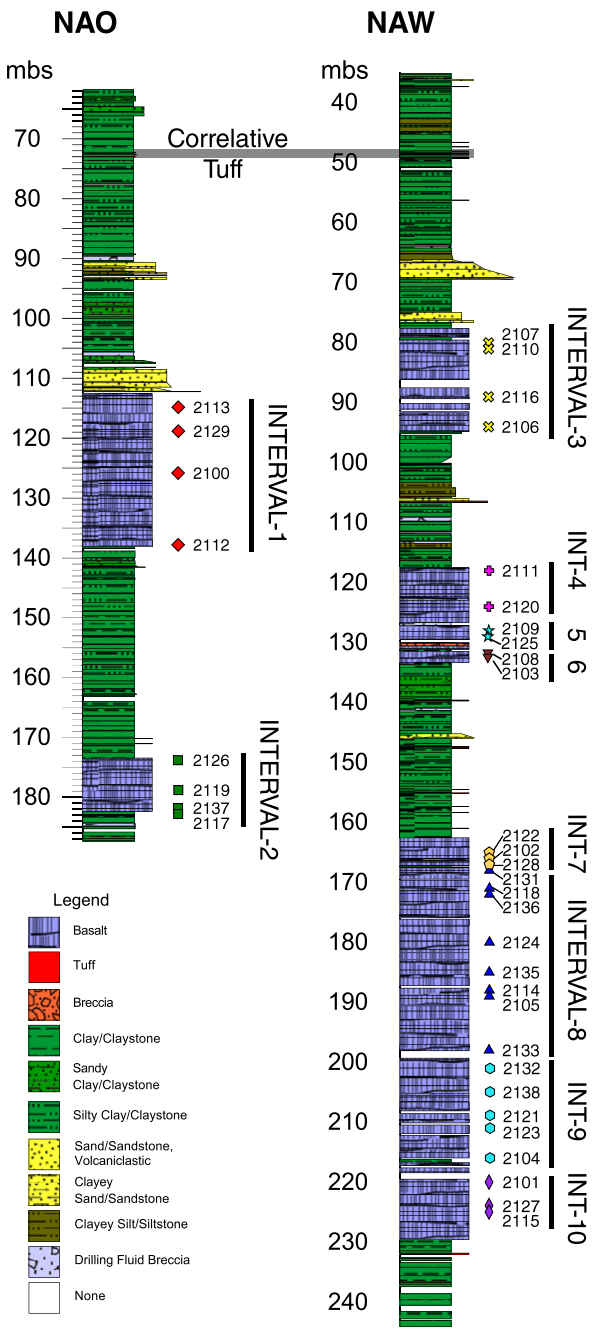

Fig. 2. Stratigraphic logs of HSPDP cores NAO and NAW (Cohen et al., 2016). The original meters below surface (mbs) for each drill core is shown along with the location of the basaltic intervals. The cores have been geochemically correlated using an airfall tuff found in both. Subsequent stratigraphic arrangement of the basaltic intervals in a single stratigraphic arrangement (Fig. 5) is made based on corrected mbs based upon this correlative tuff. Samples were taken at the drill core levels shown by the colored symbols; sample numbers are shown as 4 digit numbers beside the symbols.

texture is more common in the upper parts of the core. The petrographic characteristics of the outcrop samples are distinctly different from the core samples – being dominantly fine grained and intergranular with sparse plagioclase phenocrysts. With the exception of sample TOR0001EX (Supplemental Information), the outcrop samples do not exhibit glomeroporphyritic texture.

After sampling at the Continental Scientific Drilling Facility (formerly LacCore) at the University of Minnesota, all samples were prepared and analyzed at the Geoanalytical Lab at Michigan State University. Samples were trimmed to remove signs of visible al-

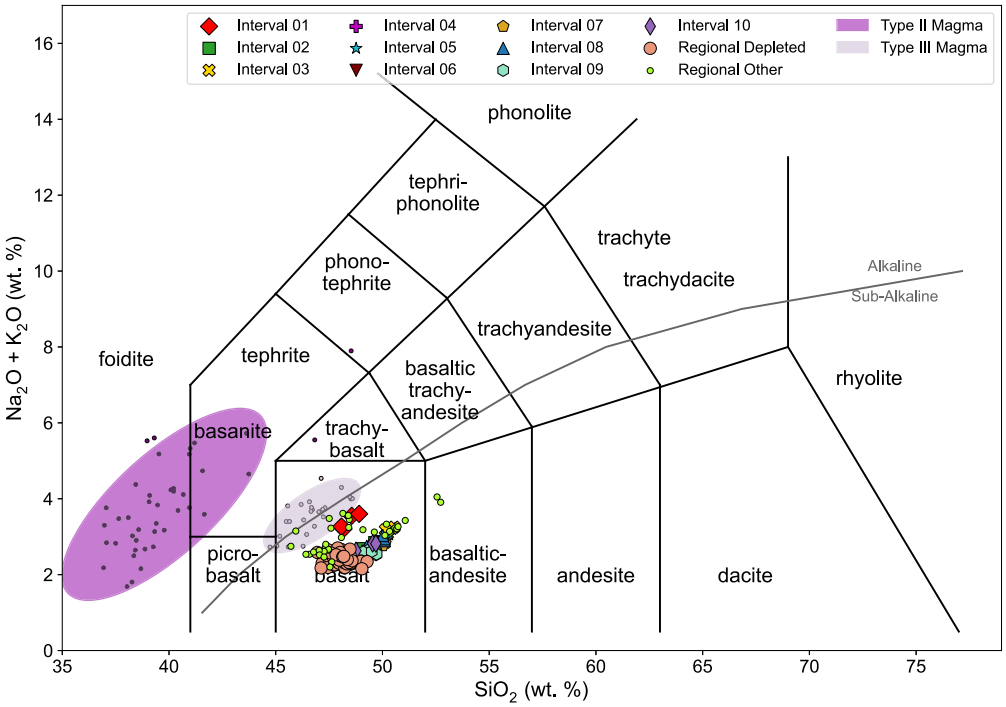

Fig. 3. Total Alkali Silica diagram showing the classification of the Afar Stratoid Series as sub-alkaline basalts. For samples from this study, we use the Interval and Outcrop names to identify material from this study and large symbols. For other Mile data (Alene et al., 2017) we have amalgamated their groups: Regional Depleted and Regional Other. These three groups are denoted by smaller symbols. The Type II magmas are the High Ti lavas from Gerba Guracha on the adjacent northwestern Ethiopian Plateau (Rooney et al., 2017). The Type III magmas are from the Pliocene Akaki field – in the northern Main Ethiopian Rift (Rooney et al., 2014a). The Type II and III data are enclosed by 2σ confidence ellipses.

teration, though given the highly vesicular texture of the samples, it was not possible to exclude all of the post-magmatic products. Samples were cut with a rock saw, polished to remove saw marks and then cleaned in reverse osmosis purified water in an ultrasonic bath. Sample billets were lightly crushed in a steel jaw crusher and then powered using a BICO UA flat plate pulverizer fitted with ceramic contamination control plates. Glass disks prepared from the powder were analyzed for major elements by x-ray fluorescence using a Bruker Pioneer S4 XRF. Analytical precision over the period of analysis is better than 1%, combined precision and accuracy is typically better than ∼2%. The same glass disks were then analyzed in triplicate for trace elements using laser-ablation inductively coupled plasma mass spectrometer (LA-ICPMS) with a Photon-Machines Analyte G2 excimer laser and Thermo Scientific ICAP Q quadrupole ICP-MS using methods described in Rooney et al. (2015). Accuracy is typically better than 5%, with the exception of Pb for which we suggest ±0.2 ppm. Analytical precision is typically better than ∼2% based on triplicate raster analysis of each disk. However, both precision and accuracy degrade closer to the limits of quantification. In this study, Rb and Cs approach these limits such that at less than 3 ppm, Rb exhibits degraded precision of up to 8% on the triplicate analysis; Cs concentrations are frequently below our limits of quantification and are thus not reported.

4. Results

We compare the data from this study with analyses of nearby Afar Stratoid Series basalts from Woranso-Mille (∼35 km away), which are dominantly older (ca. 3.8 – 3.4 Ma) (Alene et al., 2017; Saylor et al., 2019). We create two subdivisions of these existing data, clustering groups with similar geochemical characteristics: *Regional Depleted* (Am-Ado-Aralee Issie Basalt, Kerare-Burtele Basalt); *Regional Other* (Guda Basalt, Daba Dora Basalt, Gugubsi Basalt, Mile Basalt).

The core and outcrop samples from this study are uniformly defined as subalkaline basalts (Fig. 3), exhibiting major and trace element correlations with MgO that are consistent with differentiation (Fig. 4). Stratigraphically older Afar Stratoid Series basalts from Woranso-Mille are approximately within the range observed for our samples, though extend to much higher values of MgO (to nearly 10 wt.%) (Alene et al., 2017; Saylor et al., 2019). Exceptions to these correlations are: (A) Interval 3 and outcrop samples from Mile Junction. These samples exhibit significant enrichments in TiO_2, P_2O_5, and incompatible trace elements (excepting Sr) and depletion in CaO values. (B) Interval 1, which exhibits low CaO but also lower SiO_2 and significantly elevated Al_2O_3 (and is petrographically distinct).

Most first-row transition elements (e.g., V, Cr, Ni, Ga, Co) exhibit trends consistent with a model of magmatic differentiation with decreasing Ni and Cr, and increasing Ga and V with decreasing MgO (Fig. 4; Supplemental Information). However, Sc exhibits scatter and samples from Interval 1 plot at the lowest values in the series (suggestive of clinopyroxene control on fractionation within these samples). Co does not show a clear correlation with MgO within our sample suite, however samples from Interval 3 and outcrop samples from Mile Junction are notably depleted in this element compared with other Intervals of equivalent MgO.

Taken together with the major element similarities, it is likely that most samples from our field site underwent similar melt generation and differentiation processes. That is, the primary control on major and trace element variation within our dataset depends on how primitive the basalt is. Despite these similarities for the majority of the data, some differences are evident – specifically in relation to the incompatible element depleted middle stratigraphic horizon of the regional dataset. While these samples are among the most primitive, they demonstrate a parallel evolution (e.g., MgO vs Nb: Fig. 4) to other equally primitive samples from the lower and upper horizon. Notably, these samples also show particularly depleted values of Cr (Fig. 4).

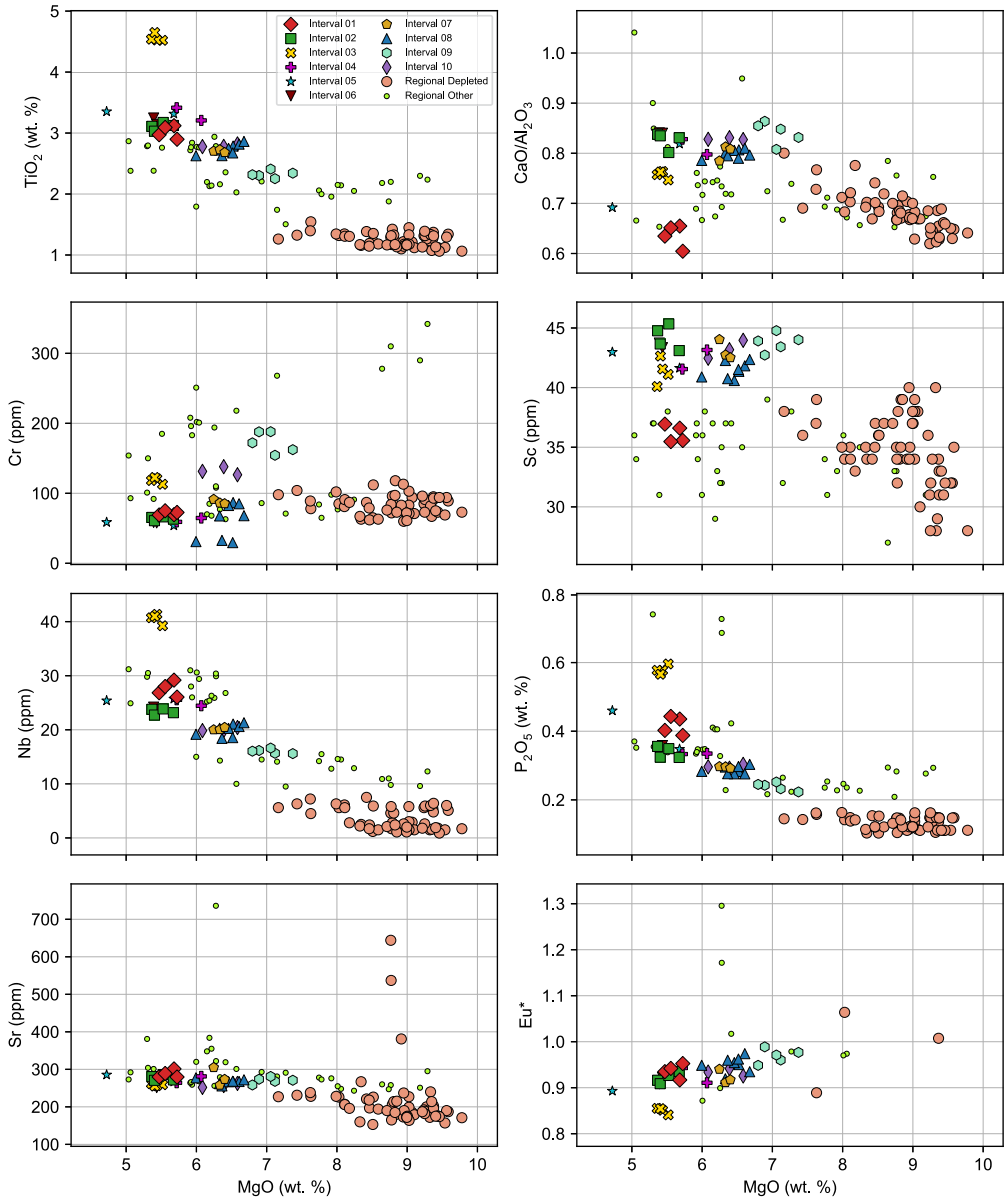

Fig. 4. Geochemical variation diagrams of Afar Stratoid Series data from Mile plotted against MgO as an index of differentiation. For samples from this study, we use the Interval and Outcrop names to identify material from this study and large symbols. For other Mile data (Alene et al., 2017) we have amalgamated their groups: Regional Depleted and Regional Other. These three groups are denoted by smaller symbols. Eu* is the europium anomaly based upon the methods of O'Neill (2016).

The stratigraphic control afforded by the HSPDP drilling project provides an unusual temporal constraint on magmatic processes active during the Pliocene in Afar. Examining data from within each of the basaltic horizons (Intervals 1 to 10), most horizons show limited (if any) evidence of intra horizon variability, consistent with a hypothesis that these horizons consist of single flows (flow boundaries are difficult to identify within a basaltic horizon in the 6.35 cm diameter core). Large ion lithophile elements exhibit some scattering of values, with Ba exhibiting the most variance, with spikes in Interval 5 and 6 from typically 100 ppm to 600 ppm (Fig. 5). Interestingly this anomaly occurs over broadly the same stratigraphic horizon (Fig. 5) and may be the result of partly-filled vesicles.

Inter-flow geochemical variability within the basalts of the NAO and NAW cores reveals some changes in the regional magmatic system through time. Core NAO has only two lava horizons – an upper 25 m thick basalt (Interval 1) and lower 9 m thick basalt (Interval 2) (Fig. 2). Both horizons contain internally homogenous basalt with ~5.5% MgO, though Interval 1 has slightly higher concentrations of the more incompatible trace elements (e.g., Nb: Fig. 5), and is quite distinct in terms of elements such as Sc, CaO and Al_2O_3 (Fig. 2; 5), suggestive of more dominant clinopyroxene fractionation.

With 8 flows, core NAW has a significantly greater volume of basalts, which can be divided into three primary cycles (separated by sediments) (Fig. 2) and are shown as colored fields in Fig. 5:

(1) The deepest cycle is ~65 m thick and comprises four identifiable intervals – Interval 7, 8, 9 and 10. Glomerophyric texture is less common in these intervals. The oldest lavas (Interval 10) form a 12 m thick layer that exhibits evidence of moderate magmatic differentiation (MgO ~6%). These lavas are overlain by a thick (30 m) horizon of more primitive lavas (MgO up to 7.3 wt.%), which also have the most depleted incompatible trace element characteristics in the study (Fig. 4). Following this horizon, there is an abrupt return to more differentiated lavas (~6 wt.% MgO) in Interval 7, 8 for about 35 m. Superficially, units in Interval 7, 8 and

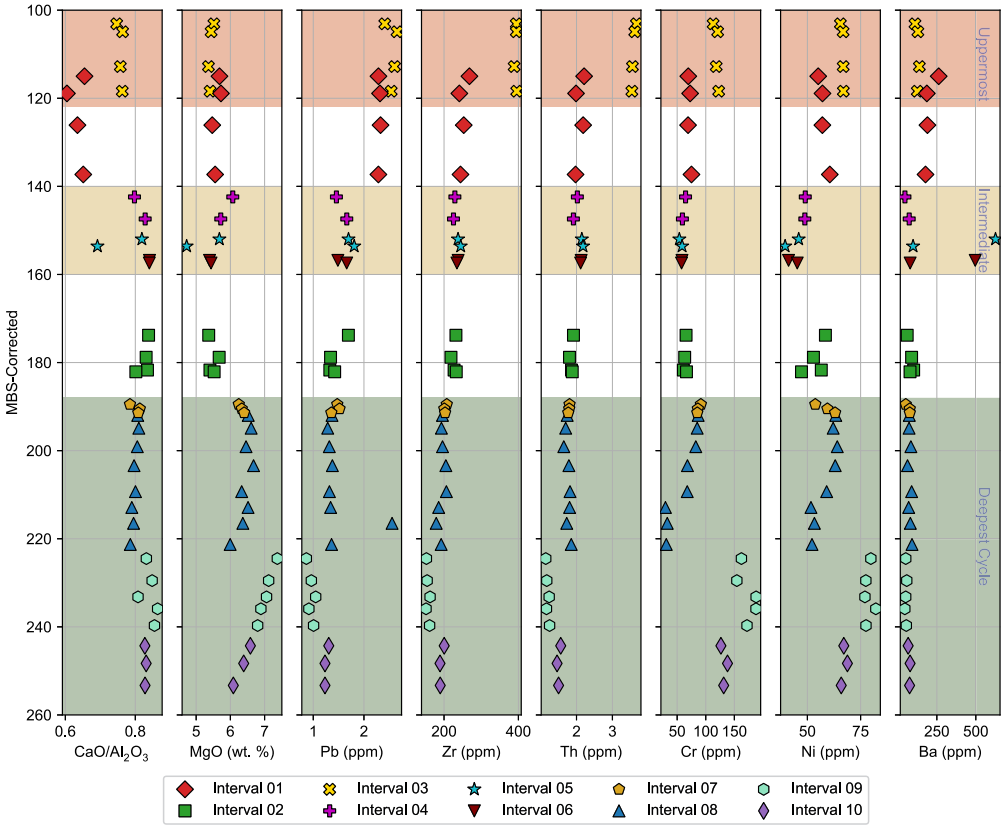

Fig. 5. Stratigraphic arrangement of geochemical data based on revised positions within the drill cores (see Fig. 2). MBS = meters below surface.

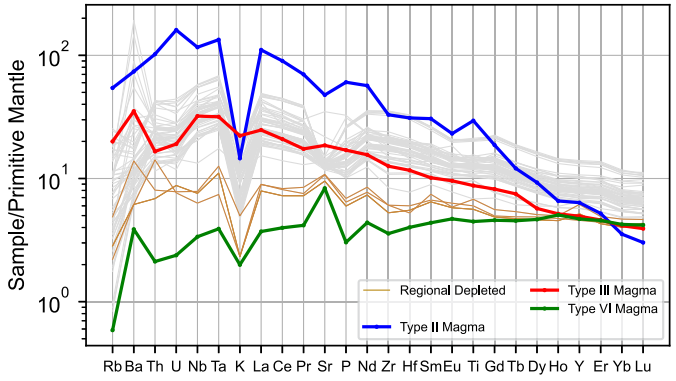

Fig. 6. Primitive mantle normalized incompatible trace element variation diagram. The normalizing values of Sun and McDonough (1989) were used. The Afar Stratoid Series lavas plotted are lavas from this study and also those of Alene et al. (2017). We have highlighted the distinctively incompatible trace element depleted values of Regional Depleted. Note the Ba anomalies in some Afar Stratoid Series lavas likely result from post-depositional processes as described in the main text. For comparison we show three magma types (Type II, III, and VI) common in Cenozoic East African magmatism (Rooney, 2020b). Most Afar Stratoid Series lavas exhibit similarities with Type II magmas, though are more depleted in the more incompatible trace elements and more enriched in the more compatible elements. The Stratoid magmas typically do not share the same pattern of Type III lavas but have similar levels of trace element enrichment. It is notable that the Type VI and Regional Depleted lavas share similarities in overall pattern. See discussion in the main text.

10 appear identical, raising the possibility that these units were derived from the same magmatic event. However, upon closer inspection, Interval 10 has lower concentrations of Th and elevated Cr, Ni compared to Intervals 7 and 8 (Fig. 5).

(2) The intermediate cycle, which is 15 m thick, is comprised of three units – Interval 4, 5 and 6, and is separated from the deepest cycle by a thick sedimentary package (~30 m). These units exhibit strong glomerophyric texture, are more evolved (5.5% MgO), and are typically thinner (3-9 m) than the deeper cycle. Interval 2 from core NAO has similar characteristics and may correlate with Intervals 4, 5, and 6 from core NAW though the absolute depths vary (Fig. 5).

(3) The uppermost magmatic cycle is a 17 m thick basaltic horizon of single composition (Interval 3) displaying larger crystal size and evidence of sub-ophitic texture. It is separated from the intermediate cycle by a 20 m sediment package. This cycle is characterized by a similar MgO content as the flows from the intermediate cycle (~5.5% MgO), however, Interval 3 has otherwise very distinctive major and trace element compositions (Fig. 5).

5. Discussion

5.1. Origin of the Afar Stratoid Series lavas

Alene et al. (2017) present a model in which the Stratoid Series lavas plot in isotopic space consistent with magma generated from a mix of plume, depleted mantle, and lithospheric reservoirs, as defined from modern magmatism in the MER (Rooney et al., 2012a). In the MER model, the mantle beneath the northern East African Rift has become contaminated with lithospheric materials, forming hybrid asthenospheric compositions. Melts derived from this hybrid asthenosphere mix with melts derived from the upwelling Afar plume and yield distinct mixing arrays between the plume and hybrid depleted mantle-lithosphere compositions (Rooney et al., 2012a; Alene et al., 2017). While the Stratoid Series plots within isotopic space consistent with the three endmember mixing model, it does not yield mixing arrays. This suggests that although the same isotopic endmembers may be involved in the formation of the Afar Stratoid Series, the mechanism of melt generation likely differs.

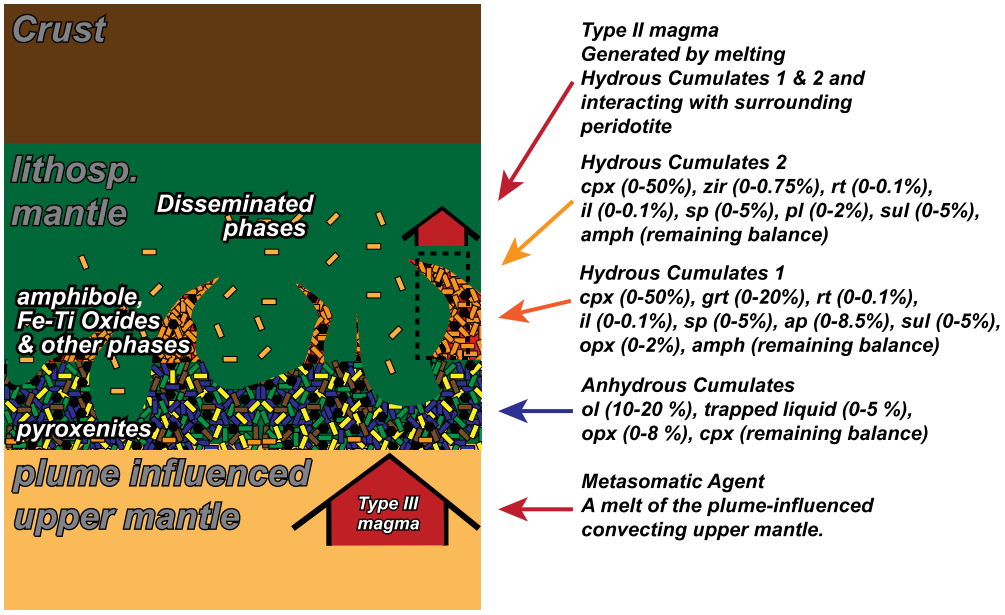

Fig. 7. Cartoon illustrating the conceptual formulation of our numerical model based on the model of Pilet et al. (2011). The initial event is the melting of the regional plume influenced upper mantle (shown in orange) to form a Type III magma. This magma percolates through the depleted continental lithospheric mantle (shown in green) as a metasomatic agent. The initial composition of the metasomatic agent is modified by the crystallization of Anhydrous Cumulates deep in the continental lithospheric mantle. We use the range of modal compositions for this cumulate as shown, recognizing the probable heterogeneity in the crystallization process. Once the metasomatic agent reaches the amphibole stability field, we modify the composition of the fractionating assemblage and remove a composition termed Hydrous Cumulate 1, which has the potential range in modal mineral compositions as shown. At higher levels within the continental lithospheric mantle, further changes to the modal mineral assemblage will result in the formation of Hydrous Cumulate 2. An average metasome composition is calculated from Hydrous Cumulates 1 and 2. Melt generated from this model metasome reacts with the surrounding depleted peridotite or mixes with a depleted melt derived from the peridotite. Mineral list: ol = olivine, opx = orthopyroxene, cpx = clinopyroxene, pl = plagioclase, grt = garnet, amph = amphibole, ap = apatite, il = ilmenite, rt = rutile, sp = sphene/titanite, sul = sulfide, zir = zircon.

Differences between the primitive-mantle normalized trace element patterns of modern magmatism in the MER and Afar and the Afar Stratoid Series at Mile support the notion of heterogeneity in melt generation mechanisms. Based on primitive-mantle normalized trace element patterns, basaltic lavas within the East African Rift System have been divided into 6 broad 'Types', which reflect their heterogeneous sources (Rooney, 2020a, 2020b). Modern basaltic magmatism in the central and northern MER exhibits trace element patterns defined by a prominent positive Ba anomaly, bracketed by a relative depletion in Rb, and Th-U (Fig. 6) – a Type III magma pattern, which is interpreted as being derived from plume-influenced upper mantle (Rooney, 2020b). Some Afar Stratoid Series lavas that are dominantly located at the edges of the sequence (northern MER and Djibouti) appear to have a Type III composition. However, the majority of the Stratoid Series lavas typically lack the positive Ba anomaly diagnostic of Type III magmas and instead display prominent negative K anomalies typical of Type II magmas (Rooney, 2020b).

Type-II magmas within the East African Rift System have been interpreted as melts of:

(i) An eclogite component convected within the Afar plume or dripped into the upper mantle, typified by the Oligocene high-titanium (HT2) Flood Basalts (e.g., Furman et al., 2016). The suggested eclogite-sourced African-Arabian HT2 flood basalts exhibit a significant fractionation in HREE that is consistent with residual garnet in their source (mean Tb/Yb_{CN} = 3.09; s.d. = 0.38). However, the HREE of the Afar Stratoid Series at Mile are relatively unfractionated (mean Tb/Yb_{CN} = 1.54; s.d. = 0.07) and inconsistent with such a source.

(ii) An ancient enriched lithospheric mantle (Rooney et al., 2014b). Magmas derived from this enriched lithospheric mantle exhibit extreme Pb isotopic compositions that require a high-μ source and a significant period of in situ radiogenic decay.

(iii) A Cenozoic aged plume-enriched lithospheric mantle (Rooney, 2020b). The interaction between plume-derived magmas with the lithospheric mantle would generate enriched domains that would have an isotopic value similar to lavas erupted today in Afar but would not preserve the pseudo-binary arrays, as is observed in the Afar Stratoid series.

Given these observations we focus on an origin for the Afar Stratoid Series lavas from the melting of a plume-enriched lithospheric mantle.

5.2. Modelling the formation and subsequent melting of a mantle metasome

Percolation of convecting mantle-derived melts through the lithospheric mantle produces co-existing silicate, carbonate, and hydrous melts that create complex lithologic domains termed 'metasomes' (e.g., Pilet et al., 2011). Important components of such metasomes are amphibole-rich veins, which generate melts compositionally equivalent to a Type II magma (Pilet et al., 2008). Exploring the potential contribution of amphibole-rich metasomes to the Afar Stratoid Series lavas requires a two-step modelling approach that firstly simulates the formation of such metasomes from a mantle-derived magma, and secondly generates melts from these metasomes (Fig. 7). To simulate this two-step process, we follow the Monte Carlo based methods of Pilet et al. (2011).

To simulate the formation of metasomes within the lithospheric mantle, we selected as potential metasomatic agents: (i) the DMM/E-DMM composition used by Pilet et al. (2011), and (ii) an East African Type III magma (Fig. 6). The DMM/E-DMM sourced magma did not yield acceptable model results (Supplemental Information). We therefore focused our modelling efforts on Type III magmas, which are melts of the convecting upper mantle (mixture of plume, lithospheric materials, and the depleted upper mantle: Rooney et al., 2012a), that are isotopically simi-

lar to the Afar Stratoid Series lavas (Alene et al., 2017). As these magmas percolate through the lithosphere, anhydrous cumulates dominated by clinopyroxene (with garnet, olivine, and orthopyroxene) are the first to crystallize (Fig. 7) (Pilet et al., 2011). At shallower depths, the crystallizing assemblage becomes dominated by amphibole (with pyroxene, garnet, phlogopite, plagioclase, rutile, ilmenite, titanite, allanite, apatite, zircon and sulfide).

Our model used the limits on modal abundances proposed by Pilet et al. (2011) with the following exceptions: (1) We increased the permitted range of modal abundances of garnet, apatite, and zircon. (2) We excluded allanite and phlogopite from the cumulate assemblage. While phlogopite is an important deep lithosphere metasomatic phase contributing to magmatism in the northern part of the Western Branch of the EARS (e.g., Rosenthal et al., 2009), it yields distinctive potassic magma compositions that are not observed away from the craton-influenced portions of the EARS (e.g., Foley et al., 2012; Rooney, 2020b) and is thus an inappropriate component in our model, which is focused on thinned mobile belt lithosphere.

The model construction of Pilet et al. (2011) acknowledges that Ti is a stoichiometrically defined component of ilmenite, rutile, and titanite, and Zr and Hf in zircon. Removal of such phases based solely upon the permitted modal ranges outlined in the model may yield negative Ti and/or Zr and Hf concentrations in the calculated residual liquid and were deemed invalid. We used modal abundance ranges to generate 50,000 possible hydrous and anhydrous metasome compositions using a Monte Carlo approach, concluding that 26,743 had valid compositions. To simulate the petrogenesis of the Afar Stratoid Series lavas, we generated a melt from the valid metasome compositions by assuming non-modal batch melting using the incongruent melting reactions of Pilet et al. (2008) until amphibole exhaustion (see Supplemental Information).

The composition of the melts produced from these models replicate the Type II magma primitive mantle normalized trace element pattern, which has been previously described as generated from a melt of metasomatized lithospheric mantle (Fig. 8a) (Rooney, 2020b). However, melts of these types of metasomes yield nepheline normative compositions (Pilet et al., 2008), distinct from the hypersthene and quartz normative subalkaline compositions typical of the Afar Stratoid Series (Fig. 3). Mixing between metasome-derived melts and magmas derived from the ambient upper mantle (i.e., Type III magmas) cannot resolve this issue: where such mixing occurs elsewhere in East Africa, it yields lavas that are typically silica undersaturated and have a trace element pattern that is inconsistent with the Afar Stratoid Series (Rooney et al., 2017; Rooney, 2020b). Alternatively, interaction between the metasome-derived melts and surrounding peridotite may provide another mechanism for modifying the melt composition. Experiments sandwiching amphibolites with peridotite have demonstrated how orthopyroxene in the peridotite is dissolved, increasing the SiO_2 content in the magma and decreasing the overall concentration of incompatible trace elements in the melt (Pilet et al., 2008). In addition, mixing between the metasome-derived melts and melts derived from the surrounding depleted peridotite would also reduce the incompatible trace element concentration of the hybrid magmas (Fig. 8b). Within the Afar Stratoid Series, there exists a wide range in incompatible trace element concentrations perhaps pointing to the operation of these processes.

Regional Depleted samples from Mile have been previously identified as having a distinctive parental magma composition that is much more depleted in incompatible trace elements (Alene et al., 2017) (Fig. 4), suggesting the influence of an additional depleted component. These samples plot central to the existing data cluster in most isotopic systems (Alene et al., 2017), ruling out an increased contribution from the depleted MORB mantle. An alternative mechanism to produce a depletion in incompatible trace elements is through mixing with an unusual LREE-depleted magma type identified in Afar (e.g., Daoud et al., 2010), which are termed Type VI magmas on the basis of the classification of Rooney (2020b). Type VI magmas exhibit much of the same incompatible trace element characteristics of MORB (Fig. 6) but have isotopic values that are more similar to Type III magmas. Accordingly, contributions from a Type VI magma would result in significant depletion of the more incompatible trace elements without imparting a corresponding depleted mantle isotopic signature. Moreover, such an interaction would resolve the pronounced Cr depletion in Regional Depleted samples (Fig. 4). Type VI lavas from nearby Mando Hararo exhibit relatively mafic compositions (8.5 wt% MgO, 101 ppm Ni) but are profoundly depleted in Cr (64 ppm) (Barrat et al., 2003); mixing between such magmas and those generated by our model could resolve the peculiar features of the Regional Depleted lavas, and more broadly, some of the depletion of incompatible trace elements inherent to the Afar Stratoid Series lavas (Fig. 8c).

Type VI magmas have been described as originating as a depleted component that is an 'intrinsic part of the Afar Plume' (Daoud et al., 2010). However, the appearance of this component in Afar, linked with regions of pronounced lithospheric thinning and melting of the lithospheric mantle, could also suggest a potential origin as a depleted component within the continental lithospheric mantle that surrounds the enriched metasomes. With the existing data it is not possible to fully resolve the origin of Type VI magmas and further study is necessary.

Using an initial composition equivalent to a melt of the current convecting upper mantle in this region (Type III magma), we can produce a metasome, which upon melting, generates a composition equivalent to a Type II magma. The interaction of this magma with the depleted mantle surrounding the metasome, and/or its melts, decreases the incompatible trace element concentration of the resulting magma.

5.3. Extensional destabilization of the lithospheric mantle

Our model of pervasive interaction between magmas and the continental lithosphere is supported by numerous seismic tomographic imaging studies that consistently reveal markedly slow shear wavespeeds (Celli et al., 2020; Chambers et al., 2022) and melt-related seismic anisotropy (e.g., Bastow et al., 2010) at lithospheric mantle depths. The mechanism of melt generation in Afar remains a topic of active debate with most focus on decompression melting of the asthenosphere (e.g., Rooney et al., 2012b; Ferguson et al., 2013; Rychert et al., 2012). We suggest that the process of continual re-enrichment by metasomatic overprint, and subsequent melting, likely contributes to the magmatism in Afar and provides an alternative mechanism for melt generation during terminal rifting.

Generation of melt from lithospheric mantle metasomes requires thermo-baric destabilization of the continental lithosphere (Rogers et al., 1998; Rooney et al., 2014b). The upper mantle beneath East Africa is anomalously hot and has been so for at least 45 Myr (Rooney et al., 2012b), thus providing a mechanism for melting of the lithospheric metasomes by modification of the conductive geotherm (e.g., Rogers et al., 1998). However, the pulsed nature of magmatism in the region implies a more discrete process. Throughout East Africa, Type II magmas are often associated with the initial extension of the continental lithosphere (Rooney, 2020b). Along the western Afar margin, structural investigations have revealed an initial stretching phase over a wide area at ca. 25 Ma, which resulted in the tilting of the Oligocene flood basalts (Wolfenden et al., 2005; Stab et al., 2016). This stretching event was contemporaneous with or immediately preceded the ca. 24-25 Ma Gerba Guracha Type-II lavas (Rooney et al., 2014b). A second mechanical extension phase in Afar is recorded between 7 and 4

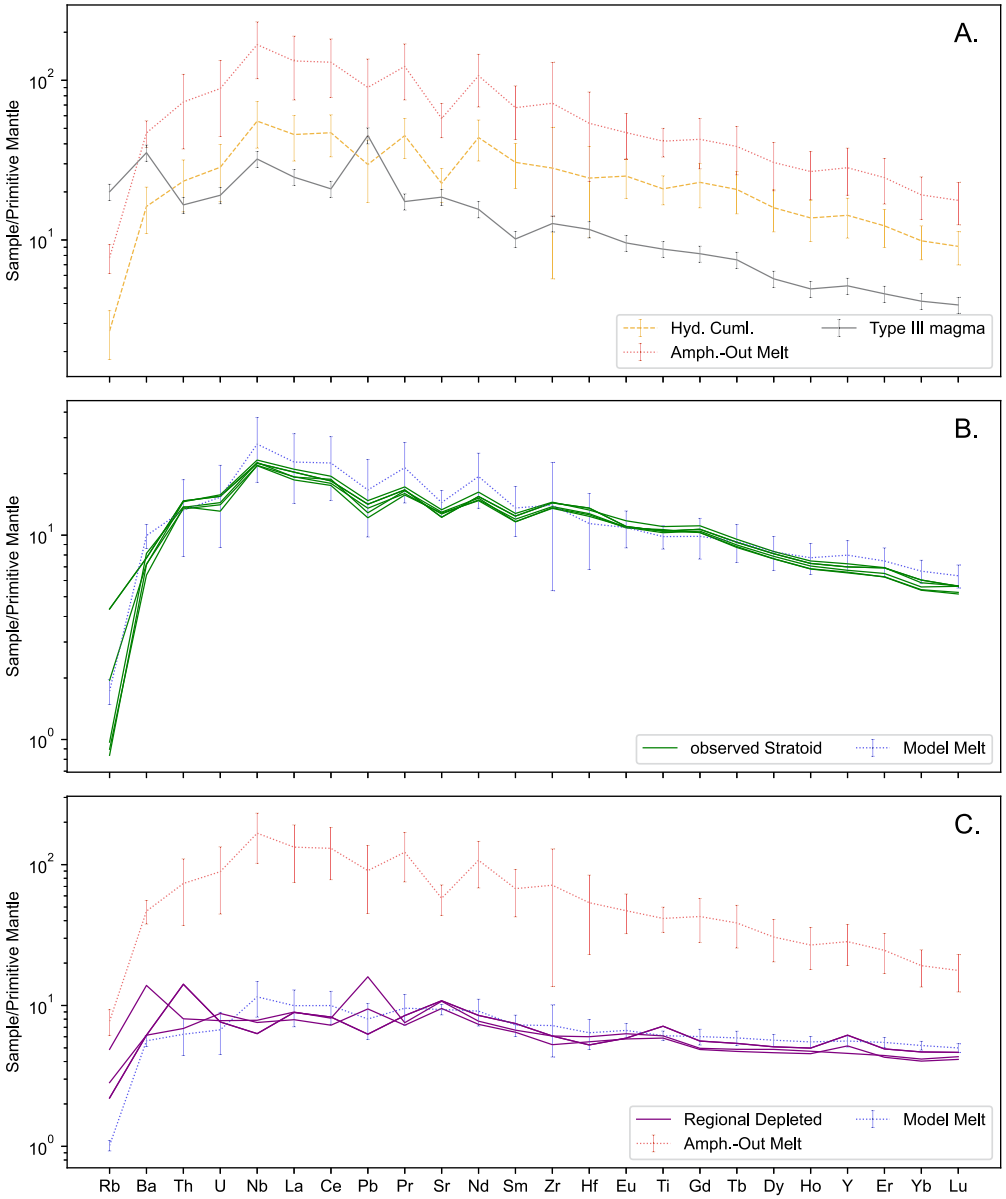

Fig. 8. Primitive mantle normalized representation of our modelling results.
A. We show the composition of the Type III magma used as the metasomatic agent (black curve). Using Monte Carlo methods, this Type III magma composition was used to create 50,000 metasomes (orange dashed curve) that were permitted to vary within the ranges noted in Fig. 7. Valid metasome compositions were then melted to amphibole exhaustion assuming non-modal batch melting using the incongruent melting reaction of Pilet et al. (2008) – see supplemental documents for more information. All error bars denote 1σ uncertainties.
B. The melts of the hydrous metasomes produced in Part A are too enriched in incompatible trace elements to be an appropriate source of the Afar Stratoid Series lavas, requiring interaction with a depleted endmember. The first mechanism that may decrease the incompatible trace element concentration in the modelled melts is a reaction between the melt and the depleted peridotite surrounding the metasome. This reaction would increase the concentration of SiO_2 in the magma and decrease the incompatible trace element concentrations (Pilet et al., 2008). An alternative process is mixing of the hydrous metasome melt with a Type VI depleted magma (See Fig. 6). We show a solution (blue dotted curve) that defines the maximum contribution required (85%) if only mixing between a Type VI magma (with 10% uncertainty added) and hydrous metasome melt is considered (though it is likely both processes contribute to the final magma composition). This model result is compared to the composition of the most primitive samples from our study (Interval 9; green curves). Error bars denote 1σ uncertainties.
C. Mixing between a hydrous metasome melt and Type VI magma (with 10% uncertainty added) to produce the Regional Depleted suite of Afar Stratoid Series magmas. This model was produced by implementing the same code and conditions as part A. The melt of the hydrous cumulate (shown on the figure) is almost identical to that in Part A – the Monte Carlo method will result in small differences between each model run. Assuming a 95% contribution from Type VI magmas to a melt of the hydrous metasome, it is possible to generate a reasonable solution matching the Regional Depleted suite. Error bars denote 1σ uncertainties.

Ma, just prior to the commencement of the Afar Stratoid Series magmatism (Wolfenden et al., 2005; Stab et al., 2016). Thus, both the Afar Stratoid Series and Gerba Guracha Type-II lavas were contemporaneous with or directly followed a period of plate thinning.

We examine the perturbation of the geotherm that might have been imposed upon the continental lithospheric mantle by a phase of lithospheric thinning. We have used a transient 1D heat conduction model to calculate the steady-state geotherm for a 100 km thick lithosphere. The temperature at the base of the lithosphere is calculated from the regional mantle potential temperature (T_P). We implement a discrete and greatly simplified episode of thinning of the continental lithosphere by stretching and/or thermal erosion in the second model step by assuming an instantaneous and uniform 20 km thinning. We implement this thinning event by setting an initial condition for the newly thinned lithosphere as being equal to the 100 km lithosphere geotherm to 79 km depth. At 80 km

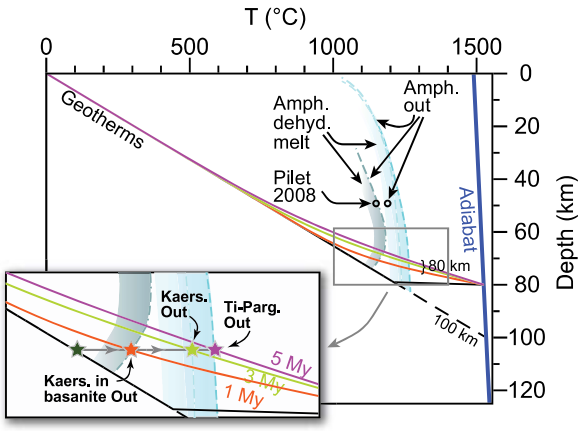

Fig. 9. 1D conductive heat model showing the steady-state geotherm for a 100 km thick lithosphere (solid and black-dashed curve), ignoring radiogenic heat production. We assume the top of the lithosphere is constrained at T=0 °C, while the temperature at the base of the lithosphere is calculated from the regional mantle potential temperature (T_P). In Afar, the maximum value of T_P = 1490 °C (Rooney et al., 2012b) translates to 1533 °C at 100 km along the adiabat. The second model step assumes an instantaneous thinning of the lithosphere to 80 km. We implement this thinning event by setting an initial condition for the newly thinned lithosphere as being equal to the 100 km lithosphere geotherm to 79 km depth. At 80 km depth, we reimposed a temperature calculated from the regional T_P such that T = 1525 °C (temperature of 1490 adiabat at 80 km depth). The transient conductive heat equation was then solved for a period of 5 million years, shown as 1 (orange), 3 (green), and 5 (purple) Myr curves. We show the results of Pilet et al. (2008) as two circles, the lower temperature circle represents the solidus for their hornblendite, while the higher temperature circle represents amphibole-out. We also show as dotted lines the amphibole-out reaction for kaersutite (Merrill and Wyllie, 1975), kaersutite in eclogite (Merrill and Wyllie, 1975), and Ti-Pargasite (Huckenholz et al., 1992). Given the lack of solidus information for these compositions, we have used the approx. melting interval of ~40 °C from the Pilet et al. (2008) experiment and added a gradient field to the lower temperature side of each of these reactions to denote that dehydration melting of amphibole should occur at temperatures lower than amphibole-out line, but that the location of the solidus is unknown. These fields have been clipped to the 100 km Geotherm. The inset is an expansion of the area within the grey box. A hypothetical amphibole-bearing cumulate is initially located beyond the amphibolite solidus (dark green star) along the 100 km geotherm. Following the modelled lithospheric thinning event, this cumulate is heated to the kaersutite-out boundary in eclogite after 1 My (orange star), the kaersutite-out boundary at 3 My (green star), and the Ti-pargasite-out boundary by 5 My. This model demonstrates that it is possible to generate melt from a hydrous cumulate located within the lithospheric mantle following a lithospheric thinning event.

depth, we reimposed a temperature calculated from the regional T_P along the adiabat. The heat equation was then solved for a time period of 5 million years. An important outcome of this hypothetical model is that hydrous cumulates generate melt following a plate thinning event (Fig. 9). These model results should be viewed as the maximum timeframe for equilibration of the mantle following a plate thinning event given the impact upon the geotherm that would be imposed by a more realistic progressive plate thinning (as opposed to instantaneous), and heat transport by magmas into the lithosphere. Despite such limitations, an important outcome of this simple model is that in a relatively short interval after plate stretching, the temperature of continental lithospheric mantle may reach the amphibolite-out boundaries assumed in our geochemical modelling. These results demonstrate that it is possible to generate melt from a hydrous cumulate located within the lithospheric mantle following a lithospheric thinning event.

5.4. Implications for magma generation during the COT

There are three existing models for generating large volumes of extrusive magmatism during the COT (listed below). These models were developed from the study of a limited number of predominately older rifted margins, and it has therefore been unclear if the melt generation mechanisms described in those models could broadly explain magmatism during the COT. Here we discuss these models in the context of the transitional environment of the northern EARS in Afar and show the existing models cannot explain the characteristics of the Afar Stratoid Series, requiring the addition of a new model for melt generation during the COT:

(1) The model of melt generation by convective upwelling of the normal asthenosphere during lithospheric thinning (e.g., Mutter et al., 1988) suggests that when extension is more focused, rapid upwelling of the mantle into the melting region is driven by high lateral temperature gradients, generating greater amounts of partial melting. In Afar, however, the modern zones of focused, 'axial', magmatism are volumetrically less significant than the more diffuse Afar Stratoid Series.

(2) High mantle potential temperatures can increase the degree of melting and volume of magma produced during the evolution of the COT (e.g., Barton and White, 1997). Elevated mantle potential temperature does play a role in melt production in Afar (e.g., Ferguson et al., 2013), but this temperature anomaly is moderate and has remained consistently elevated since the first eruption of flood basalts at ca. 45 Ma (Rooney et al., 2012b), and thus cannot explain the large volumes of magmas of the Afar Stratoid Series.

(3) Active fluxing of plume material with moderately elevated mantle potential temperature into the melting region can yield substantial volumes of melt during the COT (e.g., Fitton et al., 2000; Holbrook et al., 2001). However, the isotopic signature of Afar Stratoid series lavas does not exhibit any increased contribution from the Afar Plume component when compared to the smaller-volume modern axial volcanism within the region (Alene et al., 2017). Similarly, measures of absolute seismic wavespeed reveal relatively uniformly slow structure below the whole of Afar (e.g., Celli et al., 2020; Boyce et al., 2021).

We have shown that the process of melt generation to form the Afar Stratoid Series requires mass contribution from a recently enriched continental lithospheric mantle – a model not previously proposed for magmatism during the COT. Our conclusion is consistent with prior work on xenoliths in this region that has shown re-enrichment of the lithospheric mantle by plume-derived melts (Baker et al., 1998). We suggest that during a prior period of Cenozoic plate stretching, decompression melting of plume-influenced asthenosphere generated magmas that may have erupted along border faults or became trapped within the lithospheric mantle forming metasomes (Fig. 10a).

Our thermal modelling shows that metasomatically-enriched lithospheric mantle may become unstable as the lithosphere is stretched and thinned during rifting. As the geotherm adjusts to a thinner lithosphere, metasomatically enriched lithospheric mantle may cross its solidus resulting in magma generation (Fig. 10b). Eruption of the Afar Stratoid Series immediately followed a period of mechanical extension of the crust (Stab et al., 2016), consistent with a model of extension-related melt generation from within the metasomatically-enriched lithospheric mantle.

If the Afar Stratoid Series is considered an analog for SDRs, the mechanism of melt generation here can provide new insights into the spatial and temporal distribution of COT magmatism. The mechanisms we propose for melt generation in the Afar Stratoid Series are consistent with our view that the large volume subaerial flows necessary to create SDRs are linked with late-stage continental rifting processes (Fig. 10). A key outcome of this study is that during the continent-ocean transition the attenuation of continental lithospheric mantle may be achieved not only by stretching of the plate, but also by melting-related destruction of the continental lithospheric mantle. This model for melt generation has the appealing implication that the final stages of thinning of the continental lithosphere during COT development will coincide with an abrupt decrease in mantle melt production – a natural explanation

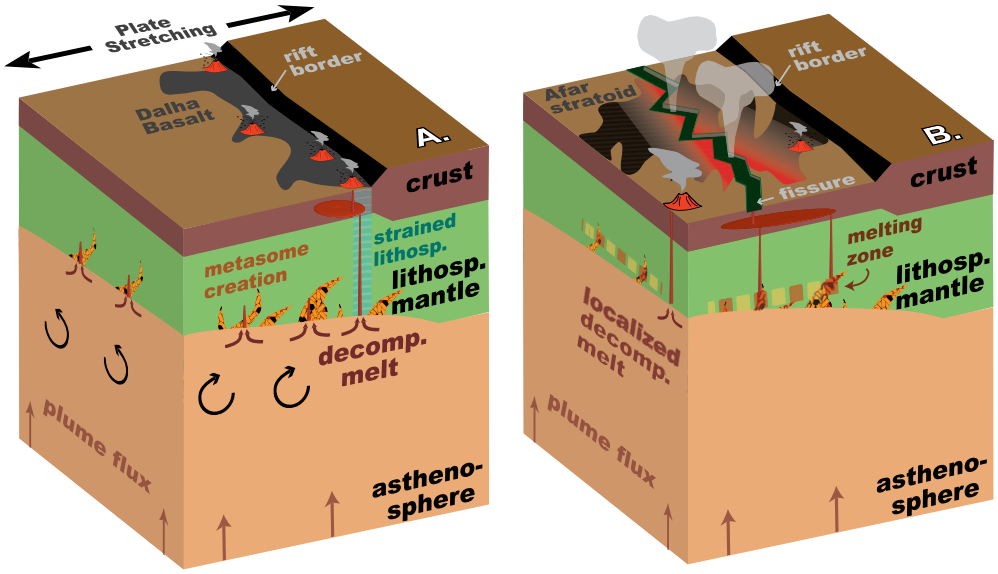

Fig. 10. Cartoon outlining the processes of metasome formation and destruction during rift evolution in Afar. A) The period denoted by this cartoon is prior to the eruption of the Afar Stratoid series, during a phase of plate stretching. During this period, thinning of the plate facilitates upwelling of the underlying mantle causing decompression melting. The melt is generated from a plume influenced upper mantle, creating a Type III magma (see main text for discussion of magma types). These Dalha Basalts preferentially erupt along the margin of the depression as magma transit is facilitated by stressed lithosphere in the region adjacent to the border faults. Magmas that do not erupt may form metasomes in the lithospheric mantle. These metasomes are shown as crystal cumulates derived from fractionation of the melt. We have not distinguished between hydrous and anhydrous cumulates in this figure. The specific time period during which the metasomes formed is not well-constrained and could have occurred throughout the Cenozoic. B) The period denoted by this cartoon is the eruption of the Afar Stratoid Series basalts. Magma is formed by destabilization of the hydrous metasomes located within the continental lithospheric mantle. Melt of the convecting upper mantle may also erupt locally given the existence of Type III magmas of the Afar Stratoid Series in the northern Main Ethiopian Rift.

for the observation that SDR sequences are lacking upon all but the very oldest oceanic crust at the edges of the ocean basins.

6. Conclusions

The Afar Stratoid Series represents the most significant magmatic event in the mature rift of the Afar Depression and exhibits characteristics consistent with SDRs – thick intercalations of laterally extensive basalts and subaerial sediments. The consistent geochemical signature of these basalts suggests a common source that is derived from plume, upper mantle, and lithospheric reservoirs. However, the trace element patterns suggest the mechanism of melt generation differs from modern axial basalts. Afar Stratoid Series lavas exhibit variability in their primitive magma compositions that suggest contributions from both incompatible element enriched and incompatible element depleted components that are isotopically similar. We constrain a model whereby melts derived from a plume-influenced convecting upper mantle continually interact with the continental lithosphere to generate metasomes. Following periods of plate thinning, perturbation of the geotherm destabilizes these metasomes, producing melts that display an incompatible element enriched Type II magma signature, but with isotopic characteristics the same as modern axial basalts (Alene et al., 2017). Interaction with the surrounding depleted peridotite decreases the incompatible trace element enrichment and increases the silica saturation (e.g., Pilet et al., 2008), yielding compositions equivalent to the observed Afar Stratoid Series lavas.

Existing models describing melt generation mechanisms to form SDRs cannot easily explain the origin of the Afar Stratoid Series. Our model provides a novel mechanism for melt generation during the COT and expands the possible modes by which SDR magmas, more broadly, might be derived. Plate thinning during the COT generates not only melts of decompressed convecting mantle, but also of enriched continental lithospheric mantle. Central to this model is the continued presence of the continental lithospheric mantle during the COT. The implication of this model is that thinning of the continental lithospheric mantle during the COT may be facilitated by both mechanical stretching, and re-enrichment and melting. The eventual destruction of the continental lithospheric mantle occurs as strain accommodation progresses from plate stretching to focused magmatic intrusion at a new oceanic spreading center, hence explaining the absence of SDRs in oceanic basins.

CRediT authorship contribution statement

Tyrone O. Rooney: Conceptualization, Data curation, Funding acquisition, Resources, Writing – original draft. **Eric L. Brown:** Methodology, Writing – review & editing. **Ian D. Bastow:** Writing – review & editing. **J Ramón Arrowsmith:** Investigation, Resources, Writing – review & editing. **Christopher J. Campisano:** Investigation, Resources, Writing – review & editing.

Declaration of competing interest

The authors declare that they have no known competing financial interests or personal relationships that could have appeared to influence the work reported in this paper.

Data availability

All new data has been provided in the article supplementary material

Acknowledgements

This work was funded by grants from the National Science Foundation (Geoprisms program OCE-1850606, EAR-1123942, EAR-1338553, BCS-1241595) and the International Continental Drilling Program (ICDP). Bastow acknowledges support from Natural Environment Research Council grant number NE/S014136/1. This is publication #53 of the Hominin Sites and Paleolakes Drilling

Project. We thank two anonymous reviewers for constructive feedback that helped improve the manuscript. We thank Rosemary Hickey-Vargas for her careful editorial handling.

Appendix A. Supplementary material

Supplementary material related to this article can be found online at https://doi.org/10.1016/j.epsl.2023.118189.

References

Alene, M., Hart, W.K., Saylor, B.Z., Deino, A., Mertzman, S., Haile-Selassie, Y., Gibert, L.B., 2017. Geochemistry of Woranso–Mille Pliocene basalts from West-central Afar, Ethiopia: implications for mantle source characteristics and rift evolution. Lithos 282, 187–200.

Baker, J., Chazot, G., Menzies, M., Thirlwall, M., 1998. Metasomatism of the shallow mantle beneath Yemen by the Afar plume - Implications for mantle plumes, flood volcanism, and intraplate volcanism. Geology 26, 431–434.

Barrat, J.A., Joron, J.L., Taylor, R.N., Fourcade, S., Nesbitt, R.W., Jahn, B.M., 2003. Geochemistry of basalts from Manda Hararo, Ethiopia: LREE-depleted basalts in Central Afar. Lithos 69, 1–13.

Barton, A.J., White, R.S., 1997. Crustal structure of Edoras Bank continental margin and mantle thermal anomalies beneath the North Atlantic. J. Geophys. Res., Solid Earth 102, 3109–3129.

Bastow, I.D., Keir, D., 2011. The protracted development of the continent-ocean transition in Afar. Nat. Geosci. 4, 248–250. https://doi.org/10.1038/Ngeo1095.

Bastow, I.D., Pilidou, S., Kendall, J.M., Stuart, G.W., 2010. Melt-induced seismic anisotropy and magma assisted rifting in Ethiopia: evidence from surface waves. Geochem. Geophys. Geosyst., Q0AB05. https://doi.org/10.1029/2010GC003036.

Boyce, A., Bastow, I., Cottaar, S., Kounoudis, R., Guilloud De Courbeville, J., Caunt, E., Desai, S., 2021. AFRP20: new P-wavespeed model for the African mantle reveals two whole-mantle plumes below East Africa and neoproterozoic modification of the Tanzania craton. Geochem. Geophys. Geosyst. 22, e2020GC009302. https://doi.org/10.1029/2020GC009302.

Brune, S., Heine, C., Clift, P.D., Pérez-Gussinyé, M., 2017. Rifted margin architecture and crustal rheology: reviewing Iberia-Newfoundland, central South Atlantic, and South China Sea. Mar. Pet. Geol. 79, 257–281.

Campisano, C.J., Cohen, A.S., Arrowsmith, J.R., Asrat, A., Behrensmeyer, A.K., Brown, E.T., Deino, A.L., Deocampo, D.M., Feibel, C.S., Kingston, J.D., 2017. The Hominin sites and Paleolakes drilling project: high-resolution paleoclimate records from the East African rift system and their implications for understanding the environmental context of hominin evolution. PaleoAnthropology 2017, 1–43. https://doi.org/10.4207/PA.2017.ART104.

Celli, N.L., Lebedev, S., Schaeffer, A.J., Gaina, C., 2020. African cratonic lithosphere carved by mantle plumes. Nat. Commun. 11, 92. https://doi.org/10.1038/s41467-019-13871-2.

Chambers, E.L., Harmon, N., Rychert, C.A., Gallacher, R.J., Keir, D., 2022. Imaging the seismic velocity structure of the crust and upper mantle in the northern East African Rift using Rayleigh wave tomography. Geophys. J. Int. 230, 2036–2055.

Cohen, A., Campisano, C., Arrowsmith, R., Asrat, A., Behrensmeyer, A.K., Deino, A., Feibel, C., Hill, A., Johnson, R., Kingston, J., 2016. The Hominin Sites and Paleolakes drilling project: inferring the environmental context of human evolution from eastern African rift lake deposits. Sci. Drill. 21, 1–16.

Daoud, M.A., Maury, R.C., Barrat, J.A., Taylor, R.N., Le Gall, B., Guillou, H., Cotten, J., Rolet, J., 2010. A LREE-depleted component in the Afar plume: further evidence from quaternary Djibouti basalts. Lithos 114, 327–336. https://doi.org/10.1016/j.lithos.2009.09.008.

DiMaggio, E.N., Arrowsmith, J.R., Campisano, C.J., Johnson, R., Deino, A.L., Warren, M., Fisseha, S., Cohen, A.S., 2015. Tephrostratigraphy and depositional environment of young (<2.94 Ma) Hadar Formation deposits at Ledi-Geraru, Afar, Ethiopia. J. Afr. Earth Sci. 112, 234–250. https://doi.org/10.1016/j.jafrearsci.2015.09.018.

Ebinger, C.J., Casey, M., 2001. Continental breakup in magmatic provinces: an Ethiopian example. Geology 29, 527–530.

Ebinger, C.J., Keir, D., Bastow, I.D., Whaler, K., Hammond, J.O., Ayele, A., Miller, M.S., Tiberi, C., Hautot, S., 2017. Crustal structure of active deformation zones in Africa: implications for global crustal processes. Tectonics 36, 3298–3332.

Ebinger, C.J., Sleep, N.H., 1998. Cenozoic magmatism throughout East Africa resulting from impact of a single plume. Nature 395, 788–791.

Eldholm, O., Gladczenko, T.P., Skogseid, J., Planke, S., 2000. Atlantic volcanic margins: a comparative study. Geol. Soc. (Lond.) Spec. Publ. 167, 411–428.

Ferguson, D.J., Maclennan, J., Bastow, I.D., Pyle, D.M., Jones, S.M., Keir, D., Blundy, J.D., Plank, T., Yirgu, G., 2013. Melting during late-stage rifting in Afar is hot and deep. Nature 499, 70–73. https://doi.org/10.1038/nature12292.

Feyissa, D.H., Kitagawa, H., Bizuneh, T.D., Tanaka, R., Kabeto, K., Nakamura, E., 2019. Transition from plume-driven to plate-driven magmatism in the evolution of the main Ethiopian rift. J. Petrol. 60, 1681–1715. https://doi.org/10.1093/petrology/egz043.

Fitton, J.G., Larsen, L.M., Saunders, A.D., Hardarson, B.S., Kempton, P.D., 2000. Palaeogene continental to oceanic magmatism on the SE Greenland continental margin at 63 N: a review of the results of Ocean Drilling Program Legs 152 and 163. J. Petrol. 41, 951–966.

Fitton, J.G., Saunders, A.D., Larsen, L.M., Hardarson, B.S., Norry, M.J., 1998. Volcanic rocks from the southest Greenland margin at 63N: composition, petrogenesis, and mantle sources. Proc. Ocean Drill. Program Sci. Results 152, 914–919. https://doi.org/10.2973/odp.proc.sr.152.233.1998.

Foley, S.F., Link, K., Tiberindwa, J.V., Barifaijo, E., 2012. Patterns and origin of igneous activity around the Tanzanian craton. J. Afr. Earth Sci. 62, 1–18.

Franke, D., 2013. Rifting, lithosphere breakup and volcanism: comparison of magma-poor and volcanic rifted margins. Mar. Pet. Geol. 43, 63–87.

Furman, T., Bryce, J.G., Rooney, T., Hanan, B.B., Yirgu, G., Ayalew, D., 2006. Heads and tails: 30 million years of the Afar plume. In: Yirgu, G., Ebinger, C., Maguire, P. (Eds.), The Afar Volcanic Province Within the East African Rift System. In: Geological Society of London Special Publication, vol. 259, pp. 95–120.

Furman, T., Nelson, W.R., Elkins-Tanton, L.T., 2016. Evolution of the East African rift: drip magmatism, lithospheric thinning and mafic volcanism. Geochim. Cosmochim. Acta 185, 418–434.

Gallahue, M.M., Stein, S., Stein, C.A., Jurdy, D., Barklage, M., Rooney, T.O., 2020. A compilation of igneous rock volumes at volcanic passive continental margins from interpreted seismic profiles. Mar. Pet. Geol. 122, 104635. https://doi.org/10.1016/j.marpetgeo.2020.104635.

Hinz, K., Neben, S., Schreckenberger, B., Roeser, H.A., Block, M., De Souza, K.G., Meyer, H., 1999. The Argentine continental margin North of 48 S: sedimentary successions, volcanic activity during breakup. Mar. Pet. Geol. 16, 1–25.

Holbrook, W.S., Kelemen, P.B., 1993. Large igneous province on the US Atlantic margin and implications for magmatism during continental breakup. Nature 364, 433–436.

Holbrook, W.S., Larsen, H.C., Korenaga, J., Dahl-Jensen, T., Reid, I.D., Kelemen, P.B., Hopper, J.R., Kent, G.M., Lizarralde, D., Bernstein, S., 2001. Mantle thermal structure and active upwelling during continental breakup in the North Atlantic. Earth Planet. Sci. Lett. 190, 251–266.

Huckenholz, H.G., Gilbert, M.C., Kunzmann, T., 1992. Stability and phase relations of calcic amphiboles crystallized from magnesio-hastingsite compositions in the 1 to 45 kbar pressure range. Neues Jahrb. Mineral. Abh. 164, 229–268.

Lahitte, P., Gillot, P.-Y., Kidane, T., Courtillot, V., Bekele, A., 2003. New age constraints on the timing of volcanism in central Afar, in the presence of propagating rifts. J. Geophys. Res., Solid Earth 108, 2123. https://doi.org/10.1029/2001jb001689.

Le Gall, B., Daoud, M.A., Maury, R., Gasse, F., Rolet, J., Jalludin, M., Caminiti, A.-M., Moussa, N., 2015. Geological Map of the Republic of Djibouti. Centre d'Etude et de Recherche de Djibouti (CERD) and CCGM.

Manatschal, G., Müntener, O., 2009. A type sequence across an ancient magma-poor ocean–continent transition: the example of the western Alpine Tethys ophiolites. Tectonophysics 473, 4–19.

Menzies, M.A., Klemperer, S.L., Ebinger, C.J., Baker, J., 2002. Characteristics of volcanic rifted margins. Spec. Pap., Geol. Soc. Am. 362, 1–14.

Merrill, R.B., Wyllie, P.J., 1975. Kaersutite and kaersutite eclogite from Kakanui, New Zealand—water-excess and water-deficient melting to 30 kilobars. Geol. Soc. Am. Bull. 86, 555–570.

Müntener, O., Manatschal, G., Desmurs, L., Pettke, T., 2010. Plagioclase peridotites in ocean–continent transitions: refertilized mantle domains generated by melt stagnation in the shallow mantle lithosphere. J. Petrol. 51, 255–294.

Mutter, J.C., Buck, W.R., Zehnder, C.M., 1988. Convective partial melting 1. A model for the formation of thick basaltic sequences during the initiation of spreading. J. Geophys. Res., Solid Earth Planets 93, 1031–1048.

Nelson, W.R., Hanan, B., Graham, D.W., Shirey, S.B., Yirgu, G., Ayalew, D., Furman, T., 2019. Distinguishing plume and metasomatized lithospheric mantle contributions to post-flood basalt volcanism on the southeastern Ethiopian Plateau. J. Petrol. 60, 1063–1094.

O'Neill, H.S.C., 2016. The smoothness and shapes of chondrite-normalized rare Earth element patterns in basalts. J. Petrol. 57, 1463–1508.

Paton, D.A., Pindell, J., McDermott, K., Bellingham, P., Horn, B., 2017. Evolution of seaward-dipping reflectors at the onset of oceanic crust formation at volcanic passive margins: insights from the South Atlantic. Geology 45, 439–442.

Pérez-Gussinyé, M., Reston, T.J., 2001. Rheological evolution during extension at nonvolcanic rifted margins: onset of serpentinization and development of detachments leading to continental breakup. J. Geophys. Res., Solid Earth 106, 3961–3975.

Peron-Pinvidic, G., et al., 2019. Rifted Margins: State of the Art and Future Challenges. Frontiers in Earth Science, vol. 7.

Peron-Pinvidic, G., Manatschal, G., Osmundsen, P.T., 2013. Structural comparison of archetypal Atlantic rifted margins: a review of observations and concepts. Mar. Pet. Geol. 43, 21–47.

Pik, R., Deniel, C., Coulon, C., Yirgu, G., Marty, B., 1999. Isotopic and trace element signatures of Ethiopian flood basalts; evidence for plume-lithosphere interactions. Geochim. Cosmochim. Acta 63, 2263–2279.

Pilet, S., Baker, M.B., Müntener, O., Stolper, E.M., 2011. Monte Carlo simulations of metasomatic enrichment in the lithosphere and implications for the source of alkaline basalts. J. Petrol. 52, 1415–1442. https://doi.org/10.1093/petrology/egr007.

Pilet, S., Baker, M.B., Stolper, E.M., 2008. Metasomatized Lithosphere and the Origin of Alkaline Lavas. Science 320, 916–919. https://doi.org/10.1126/science.1156563.

Ritsema, J., Deuss, A., van Heijst, H.J., Woodhouse, J.H., 2011. S40RTS: a degree-40 shear-velocity model for the mantle from new Rayleigh wave dispersion, teleseismic traveltime and normal-mode splitting function measurements. Geophys. J. Int. 184, 1223–1236. https://doi.org/10.1111/j.1365-246X.2010.04884.x.

Rogers, N.W., James, D., Kelley, S.P., de Mulder, M., 1998. The generation of potassic lavas from the eastern Virunga Province, Rwanda. J. Petrol. 39, 1223–1247.

Rooney, T.O., 2020a. The Cenozoic magmatism of East Africa: Part IV–the terminal stages of rifting preserved in the Northern East African rift system. Lithos, 105381. https://doi.org/10.1016/j.lithos.2019.105381.

Rooney, T.O., 2020b. The Cenozoic magmatism of East Africa: Part V–magma sources and processes in the East African rift. Lithos 360, 105296. https://doi.org/10.1016/j.lithos.2019.105296.

Rooney, T.O., 2017. The Cenozoic magmatism of East-Africa: Part I—flood basalts and pulsed magmatism. Lithos 286, 264–301.

Rooney, T.O., Bastow, I.D., Keir, D., Mazzarini, F., Movsesian, E., Grosfils, E.B., Zimbelman, J.R., Ramsey, M.S., Ayalew, D., Yirgu, G., 2014a. The protracted development of focused magmatic intrusion during continental rifting. Tectonics 33, 875–897. https://doi.org/10.1002/2013TC003514.

Rooney, T.O., Hanan, B.B., Graham, D.W., Furman, T., Blichert-Toft, J., Schilling, J.-G., 2012a. Upper mantle pollution during afar plume–continental rift interaction. J. Petrol. 53, 365–389. https://doi.org/10.1093/petrology/egr065.

Rooney, T.O., Herzberg, C., Bastow, I.D., 2012b. Elevated mantle temperature beneath East Africa. Geology 40, 27–30. https://doi.org/10.1130/g32382.1.

Rooney, T.O., Morell, K.D., Hidalgo, P., Fraceschi, P., 2015. Magmatic consequences of the transition from orthogonal to oblique subduction in Panama. Geochem. Geophys. Geosyst. 16, 4178–4208. https://doi.org/10.1002/2015gc006150.

Rooney, T.O., Nelson, W.R., Ayalew, D., Hanan, B., Yirgu, G., Kappelman, J., 2017. Melting the lithosphere: metasomes as a source for mantle-derived magmas. Earth Planet. Sci. Lett. 461, 105–118. https://doi.org/10.1016/j.epsl.2016.12.010.

Rooney, T.O., Nelson, W.R., Dosso, L., Furman, T., Hanan, B., 2014b. The role of continental lithosphere metasomes in the production of HIMU-like magmatism on the northeast African and Arabian plates. Geology 42, 419–422. https://doi.org/10.1130/g35216.1.

Rosenthal, A., Foley, S.F., Pearson, D.G., Nowell, G.M., Tappe, S., 2009. Petrogenesis of strongly alkaline primitive volcanic rocks at the propagating tip of the western branch of the East African rift. Earth Planet. Sci. Lett. 284, 236–248. https://doi.org/10.1016/j.epsl.2009.04.036.

Rychert, C.A., Hammond, J.O.S., Harmon, N., Michael Kendall, J., Keir, D., Ebinger, C., Bastow, I.D., Ayele, A., Belachew, M., Stuart, G., 2012. Volcanism in the Afar rift sustained by decompression melting with minimal plume influence. Nat. Geosci. 5, 406–409.

Saylor, B.Z., Gibert, L., Deino, A., Alene, M., Levin, N.E., Melillo, S.M., Peaple, M.D., Feakins, S.J., Bourel, B., Barboni, D., 2019. Age and context of mid-Pliocene hominin cranium from Woranso-Mille, Ethiopia. Nature 573, 220–224.

Stab, M., Bellahsen, N., Pik, R., Quidelleur, X., Ayalew, D., Leroy, S., 2016. Modes of rifting in magma-rich settings: tectono-magmatic evolution of Central Afar. Tectonics 35, 2–38. https://doi.org/10.1002/2015tc003893.

Sun, S.-s., McDonough, W.F., 1989. Chemical and isotopic systematics of oceanic basalts: implications for mantle composition and processes. In: Saunders, A.D. (Ed.), Magmatism in the Ocean Basins. In: Geological Society of London Special Publication, vol. 42, pp. 313–345.

Varet, J., 2017. Geology of Afar (East Africa). Springer.

White, R.S., Spence, G.D., Fowler, S.R., McKenzie, D.P., Westbrook, G.K., Bowen, A.N., 1987. Magmatism at rifted continental margins. Nature 330, 439–444.

Whitmarsh, R.B., Manatschal, G., Minshull, T.A., 2001. Evolution of magma-poor continental margins from rifting to seafloor spreading. Nature 413, 150–154.

Wolfenden, E., Ebinger, C., Yirgu, G., Renne, P.R., Kelley, S.P., 2005. Evolution of a volcanic rifted margin: Southern Red Sea, Ethiopia. Geol. Soc. Am. Bull. 117, 846–864.